Journal of Thermal Analysis and Calorimetry (2022) 147:1561–1570
https://doi.org/10.1007/s10973-020-10432-4

# Influence of $MWCNT/Fe_3O_4$ hybrid nanoparticles on an exponentially porous shrinking sheet with chemical reaction and slip boundary conditions

K. Swain[1] · Fateh Mebarek-Oudina[2] · S. M. Abo-Dahab[3,4]

Received: 28 May 2020 / Accepted: 23 November 2020 / Published online: 7 January 2021



## Abstract

Hybrid nanofluids are of great importance in the field of industry due to high effective thermal conductivity which causes high rates of heat transfer. The current article investigates the impact of variable magnetic field and chemical reaction of $MWCNT/Fe_3O_4$–water hybrid nanofluid over an exponentially shrinking porous sheet with slip boundary conditions. Suitable transformations convert the governing equations into coupled nonlinear ordinary differential equations. Further, these equations are solved by the help of shooting technique. The influences of operating parameters on the flow domain as well as force coefficients and rates of heat and mass transfers are computed and shown through graphs and tables. It is found that hybridity augments the temperature and concentration profiles. Further, suction/injection parameter enriches the skin friction coefficient, but reverse trend is observed for velocity slip parameter.


**Keywords** $MWCNT/Fe_3O_4$ nanoparticles · Variable magnetic field · Exponential shrinking sheet · Variable heat source/sink · Chemical reaction

## Abbreviations

| | |
|---|---|
| $x, y$ | Cartesian coordinate system (m) |
| $u, v$ | Velocity components along $x, y$ directions, respectively (m s$^{-1}$) |
| $\mu_{hnf}$ | Viscosity of the hybrid nanofluid (kg m$^{-1}$ s$^{-1}$) |
| $v_{hnf}$ | Kinetic velocity of the hybrid nanofluid (m$^2$ s$^{-1}$) |
| $v_f$ | Kinematic viscosity of the base fluid (m$^2$ s$^{-1}$) |
| $(\rho c_p)_{hnf}$ | Specific heat capacitance of the hybrid nanofluid (J kg$^{-1}$ K$^{-1}$) |
| $(\rho c_p)_f$ | Heat capacity of foundation liquid (J kg$^{-1}$ K$^{-1}$) |
| $k_{hnf}$ | Thermal conductivity of the nanofluid (m$^2$ s$^{-1}$) |
| $k_f$ | Thermal conductivity of the base fluid (m$^2$ s$^{-1}$) |
| $Kp^*$ | Permeability of the porous medium |
| $k_s$ | Thermal conductivity of the solid nanoparticle (m$^2$ s$^{-1}$) |
| $\rho_{nf}$ | Density of nanofluid (kg m$^{-3}$) |
| $\rho_f$ | Density of base fluid (kg m$^{-3}$) |
| $\rho_s$ | Density of solid nanoparticle (kg m$^{-3}$) |
| $Q_0$ | Positive constant |
| Pr | Prandtl number |
| $Kc^*$ | Reaction rate of the solute |
| $Kc$ | Chemical reaction parameter |
| $q$ | Heat source/sink coefficient |
| Sc | Schmidt number |
| $R$ | Radiation parameter |
| $D_B$ | Brownian motion coefficient (m$^2$ s$^{-1}$) |
| $S$ | Suction/injection parameter |
| $B$ | Velocity slip parameter |
| $D$ | Thermal slip parameter |
| $E$ | Solutal slip parameter |
| $T$ | Temperature (°C) |
| $T_w$ | Variable temperature at the sheet |
| $T_\infty$ | Free stream temperature (°C) |
| $C$ | Concentration |
| $Kp$ | Permeability parameter |
| $\phi$ | Dimensionless nanoparticle volume fraction |
| $C_w$ | Variable concentration at the sheet |

✉ Fateh Mebarek-Oudina
oudina2003@yahoo.fr; f.mebarek_oudina@univ-skikda.dz

[1] Department of Mathematics, Gandhi Institute for Technology, Bhubaneswar, Odisha 752054, India

[2] Department of Physics, Faculty of Sciences, University of 20 août 1955-Skikda, Road El-Hadaeik, B.P. 26, 21000 Skikda, Algeria

[3] Department of Mathematics, Faculty of Science, South Valley University, Qena 83523, Egypt

[4] Department of Computer Science, Faculty of Computers and Information, Luxor University, Luxor, Egypt

| | |
|---|---|
| $C_\infty$ | Free stream concentration |
| $f$ | Dimensionless velocity |
| $\theta$ | Dimensionless temperature |
| $\varphi$ | Dimensionless concentration |
| $C_f$ | Local skin friction coefficient |
| $Nu_x$ | Local Nusselt number |
| $Sh_x$ | Local Sherwood number |

## Introduction

Significant applications are made on shrinking sheet in manufacturing and technological processes. Fang and Zhang [1] found the particular solution for the flow over a shrinking sheet. Bhattacharyya [2] and Mukhopadhyay [3] established the dual solutions past an exponentially shrinking sheet. Nadeem et al. [4] have examined the flow behavior of water-based nanofluid. Swain et al. [5] have studied the viscoelastic nanofluid flow over an elongating sheet. Numerical simulation was made by Motsumi and Makinde [6] to study the dissipation on chemically reactive nanofluid. Naramgari and Sulochana [7] illustrated a numerical solution to study the impact of suction/injection on MHD nanofluid flow over a permeable elongating/shrinking sheet. The slip flow investigation on stretching sheet was carried out by Swain et al. [8].

Nanofluid is used to augment the heat transfer rate of base fluids. The nanoparticles are emerged in base fluid to enhance the thermal conductivity which allows more heat transfer. Hady et al. [9] have considered the nanofluid over a non-linearly extending sheet. Sheikholeslami et al. [10] obtained a numerical simulation of MHD nanofluid flow considering viscous dissipation. Mahanthesh et al. [11] explored the three dimensional flow of nanofluid over a non-linearly elongating sheet by taking water as base fluid. Ghosh and Mukhopadhyay [12] studied the slip flow analysis of two kinds of nanofluids over an exponentially enlarging sheet. Mebarek-Oudina [13] examined the nanofluid flow using different base fluids. Kolsi et al. [14] have numerical investigated the aggregation effects on *MWCNT*–water nanofluid. Ghosh and Mukhopadhyay [15] have obtained a stability analysis for nanofluid flow with slip boundary conditions. Various recent researches are carried out using analytical and numerical methods to treat heat transfer and nanofluids in thermal and energy systems [16–26].

Hybrid nanofluid is a mixture of two types of nanoparticles suspended in regular fluid and applied in all fields of heat transfer such as manufacturing, electro- and biosensors, and acoustics. Hayat and Nadeem [27] have studied the impact of heat transfer of Ag–CuO/water hybrid nanofluid over an extending sheet. Ghadikolaei et al. [28] have considered nanoparticles shape factor to study the behavior of $TiO_2$–CuO/ethylene glycol–water hybrid nanofluid over rotating cone. Waini et al. [29] have numerically examined the hybrid nanofluid flow over a nonlinear permeable enlarging/shrinking sheet. Bagheri et al. [30] have analyzed the sensitive analysis of hybrid nanofluids with consideration of heat flux. The effect of viscous dissipation on Cu–$Al_2O_3$–$H_2O$ hybrid nanofluid over a shrinking surface with stability analysis is considered by Lund et al. [31]. Aziz et al. [32] and Lund et al. [33] have investigated the hybrid nanofluid over a widening sheet. Some related investigations can be found in the articles [34–40].

Sundar et al. [41] studied the heat transfer and friction factor of MWCNT–$Fe_3O_4$/water hybrid nanofluids. Sohail et al. [42, 43] have studied the 3D flow of nanofluid over a stretching sheet with thermal radiation. Further, Sohail et al. [44–46] examined the flow of nanofluid by using different fluid model in the presence of bio-convective gyrotactic microorganisms and variable thermal conductivity. Shah et al. [47] studied the effect of Lorentz force on solidification of NEPCM. Moreover, Shah et al. [48] and Wakif [49] investigated the influences of chemical reaction on MHD Casson nanofluid over a stretching sheet. Shah et al. [50, 51] studied the micropolar Casson fluid over a stretching/shrinking sheet and between two rotating parallel plates, respectively. Deebani et al. [52] examined the Hall current effect on radiative Casson fluid with chemical reaction. Senapati et al. [53] numerical studied the three-dimensional flow of Casson nanofluid past an exponentially stretching sheet. Wakif et al. [54, 55] studied the influence of uniform transverse magnetic field on water-based nanofluids with metallic nanoparticles using Buongiorno's model. Further, Wakif et al. [56] examined the dissipative flow of Stokes second problem. Wakif et al. [57] carried out the numerical solution of unsteady Couette nanofluid flow in the existence of thermal radiation.

To the authors information, no studies have been done for flow, heat, and mass transfer characteristics of MWCNT/$Fe_3O_4$–water hybrid nanofluid over an exponentially shrinking in presence of porous matrix with slip boundary conditions. Further, the influences of thermal radiation and heat generation on chemically reactive species hybrid nanofluid are highly affected with heat transfer development theory. The efficient shooting technique is applied to solve the nonlinear ordinary differential equations (ODEs). The effects of various relevant parameters are shown through graphs and tables. It is concluded that the external new parameters such as slip parameters, Schmidt number, chemical reaction, Prandtl number, and thermal radiation make a significant impact on the hybridity which improves the temperature and concentration profiles.

## Mathematical formulation

Consider two dimensional (2D) flow of MWCNT/$Fe_3O_4$–water hybrid nanoliquid over an exponentially shrinking sheet embedded in a porous matrix. The plate is placed along *x*-axis, and a variable magnetic field $B = B_0 e^{\frac{x}{L}}$ is induced in the flow (Fig. 1). The gravitational effect and viscous dissipative heat are also neglected. The leading equations of flow, heat, and mass transport following Ghosh and Mukhopadhyay [15] and Waini et al. [59] are written as

$$\frac{\partial u}{\partial x} + \frac{\partial u}{\partial y} = 0, \tag{1}$$

$$u\frac{\partial u}{\partial x} + v\frac{\partial u}{\partial y} = \upsilon_{hnf}\frac{\partial^2 u}{\partial y^2} - \frac{\sigma_{hnf}B^2 u}{\rho_{hnf}} - \frac{\mu_{hnf}u}{\rho_{hnf}Kp^*}, \tag{2}$$

$$u\frac{\partial T}{\partial x} + v\frac{\partial T}{\partial y} = \frac{k_{hnf}}{(\rho c_p)_{hnf}}\frac{\partial^2 T}{\partial y^2} + \frac{16\sigma^* T_\infty^3}{3k^*(\rho c_p)_{hnf}}\frac{\partial^2 T}{\partial y^2} + \frac{Q}{(\rho c_p)_{hnf}}(T - T_\infty), \tag{3}$$

$$u\frac{\partial C}{\partial x} + v\frac{\partial C}{\partial y} = D_B\frac{\partial^2 C}{\partial y^2} - Kc^*(C - C_\infty), \tag{4}$$

with the corresponding boundary conditions as:

$$u = -U_w + B'\upsilon_f\frac{\partial u}{\partial y}, v = -v_w = -v_0 e^{\frac{x}{2L}},$$
$$T = T_w + D'\frac{\partial T}{\partial y}, C = C_w + E'\frac{\partial C}{\partial y} \text{ at } y = 0,$$
$$u \to 0, T \to T_\infty, C \to C_\infty \text{ at } y \to \infty, \tag{5}$$

where $U_W = -ce^{\frac{x}{L}}$ is the shrinking velocity with shrinking constant $c > 0$, and $v_w = v_0 e^{\frac{x}{2L}}$ where $v_0$ is a constant ($v_0 > 0$ indicates suction and $v_0 < 0$ indicates injection), $T_w = T_\infty + T_0 e^{\frac{x}{2L}}$ ($T_0$ is a constant), $C_w = C_\infty + C_0 e^{\frac{x}{2L}}$ ($C_0$ is a constant), $Q = Q_0 e^{\frac{x}{L}}$ are, respectively, the variable temperature, concentration and heat source/sink. Here $B' = B_1 e^{-\frac{x}{2L}}$, $D' = D_1 e^{-\frac{x}{2L}}$, and $E' = E_1 e^{-\frac{x}{2L}}$ are the velocity, thermal, and solutal slip factors, respectively.

The effective nanofluid properties are given by

$$\mu_{hnf} = \frac{\mu_f}{(1 - \phi_{MWCNT} - \phi_{Fe_3O_4})^{2.5}}, \rho_{hnf} = (1 - \phi_{MWCNT} - \phi_{Fe_3O_4})\rho_f + \phi_{MWCNT}\rho_{MWCNT} + \phi_{Fe_3O_4}\rho_{Fe_3O_4},$$
$$(\rho c_p)_{hnf} = (1 - \phi_{MWCNT} - \phi_{Fe_3O_4})(\rho c_p)_f + \phi_{MWCNT}(\rho c_p)_{MWCNT} + \phi_{Fe_3O_4}(\rho c_p)_{Fe_3O_4},$$
$$\frac{\sigma_{hnf}}{\sigma_f} = \left[1 + \frac{3\left(\frac{\sigma_{MWCNT}+\sigma_{Fe_3O_4}}{\sigma_f} - 1\right)(\phi_{MWCNT} + \phi_{Fe_3O_4})}{\left(\frac{\sigma_{MWCNT}+\sigma_{Fe_3O_4}}{\sigma_f} + 2\right) - \left(\frac{\sigma_{MWCNT}+\sigma_{Fe_3O_4}}{\sigma_f} - 1\right)(\phi_{MWCNT} + \phi_{Fe_3O_4})}\right],$$
$$\frac{k_{hnf}}{k_f} = \frac{\left[\frac{\phi_{MWCNT}k_{MWCNT}+\phi_{Fe_3O_4}k_{Fe_3O_4}}{\phi_{MWCNT}+\phi_{Fe_3O_4}} + 2k_f + 2(\phi_{MWCNT}k_{MWCNT} + \phi_{Fe_3O_4}k_{Fe_3O_4}) - 2(\phi_{MWCNT} + \phi_{Fe_3O_4})k_f\right]}{\left[\frac{\phi_{MWCNT}k_{MWCNT}+\phi_{Fe_3O_4}k_{Fe_3O_4}}{\phi_{MWCNT}+\phi_{Fe_3O_4}} + 2k_f - (\phi_{MWCNT}k_{MWCNT} + \phi_{Fe_3O_4}k_{Fe_3O_4}) + (\phi_{MWCNT} + \phi_{Fe_3O_4})k_f\right]}$$

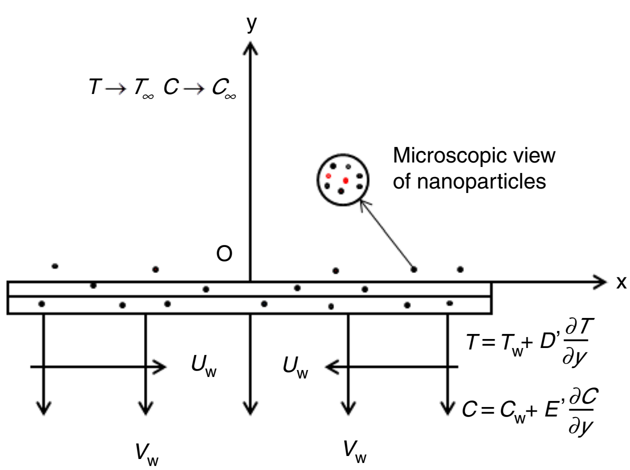


**Fig. 1** Flow geometry

where $\phi$ is the solid volume fraction, $\mu_f$ and $\mu_{hnf}$ are the dynamic viscosities, $\upsilon_f$ and $\upsilon_{hnf}$ are the kinematic viscosities, $\rho_f$ and $\rho_{hnf}$ are the densities, $(\rho c_p)_f$ and $(\rho c_p)_{hnf}$ are the heat capacitances, $k_f$ and $k_{hnf}$ are the thermal conductivities, and $\sigma_f$ and $\sigma_{hnf}$ are the electrically conductivities of the base fluid and hybrid nanofluid, respectively.

## Similarity transformations

Consider the following similarity transformation

$$\psi = \sqrt{2\upsilon_f cL}e^{\frac{x}{2L}} f(\eta), \eta = y\sqrt{\frac{c}{2\upsilon_f L}}e^{\frac{x}{2L}},$$
$$\theta(\eta) = \frac{T - T_\infty}{T_w - T_\infty}, \Phi(n) = \frac{C - C_\infty}{C_w - C_\infty}. \tag{6}$$

In view of (6), Eqs. (1)–(5) become

$$\zeta_1\zeta_2 f''' + ff'' - 2f'^2 - \zeta_2\zeta_3 Mf' - \zeta_1\zeta_2 Kpf' = 0, \tag{7}$$

$$\zeta_4\left\{\frac{k_{hnf}}{k_f} + \frac{4}{3}R\right\}\theta'' + \Pr\{f\theta' - f'\theta + q\zeta_4\theta\} = 0, \tag{8}$$

$$\Phi'' + \mathrm{Sc}\{f\Phi' - f'\Phi - \mathrm{Kc}\Phi\} = 0. \tag{9}$$

$$f(\eta) = S,\ f'(\eta) = -1 + Bf''(\eta),$$
$$\theta(\eta) = 1 + D\theta'(\eta),\quad \Phi(\eta) = 1 + E\Phi'(\eta) \text{ at } \eta = 0$$
$$f'(\eta) \to 0,\ \theta(\eta) \to 0,\ \Phi(\eta) \to 0 \text{ as } \eta \to \infty \tag{10}$$

where

$$\zeta_1 = \frac{1}{\left(1 - \phi_{MWCNT} - \phi_{Fe_3O_4}\right)^{2.5}},\ \zeta_2 = \frac{1}{\left(1 - \phi_{MWCNT} - \phi_{Fe_3O_4}\right) + \phi_{MWCNT}\left(\frac{\rho_{MWCNT}}{\rho_f}\right) + \phi_{Fe_3O_4}\left(\frac{\rho_{Fe_3O_4}}{\rho_f}\right)},$$
$$\zeta_3 = 1 + \frac{3\left(\frac{\sigma_{MWCNT}+\sigma_{Fe_3O_4}}{\sigma_f} - 1\right)\left(\phi_{MWCNT} + \phi_{Fe_3O_4}\right)}{\left(\frac{\sigma_{MWCNT}+\sigma_{Fe_3O_4}}{\sigma_f} + 2\right) - \left(\frac{\sigma_{MWCNT}+\sigma_{Fe_3O_4}}{\sigma_f} - 1\right)\left(\phi_{MWCNT} + \phi_{Fe_3O_4}\right)}, M = \frac{2LB_0^2\sigma_f}{c\rho_f}, Kp = \frac{2L\upsilon_f}{cKp^*},$$
$$\zeta_4 = \frac{1}{\left(1 - \phi_{MWCNT} - \phi_{Fe_3O_4}\right) + \phi_{MWCNT}\frac{(\rho c_p)_{MWCNT}}{(\rho c_p)_f} + \phi_{Fe_3O_4}\frac{(\rho c_p)_{Fe_3O_4}}{(\rho c_p)_f}}, S = -\frac{v_0}{\sqrt{(\upsilon_f c)/2L}}, B = B_1\sqrt{\frac{c\upsilon_f}{2L}},$$
$$D = D_1\sqrt{\frac{c}{2\upsilon_f L}}, E = E_1\sqrt{\frac{c}{2\upsilon_f L}}, R = \frac{4\sigma^* T_\infty^3}{3k_f k^*}, Q = \frac{2LQ^*}{c\left(\rho C_p\right)_f}, \Pr = \frac{\upsilon_f\left(\rho C_p\right)_f}{k_f}, \mathrm{Sc} = \frac{\upsilon_f}{D_B}.$$

The surface conditions of practical interest such as the skin friction coefficient ($C_f$), Nusselt number $\left(\mathrm{Nu}_x\right)$, and Sherwood number $\left(\mathrm{Sh}_x\right)$ are given by

$$C_f = \frac{\mu_{hnf}}{\rho_f U_w^2 e^{\frac{2x}{L}}}\left.\frac{\partial u}{\partial y}\right|_{y=0}, \mathrm{Nu}_x = -\frac{xk_{hnf}}{k_f(T_w - T_\infty)}\left.\frac{\partial T}{\partial y}\right|_{y=0} \text{ and } \mathrm{Sh}_x = -\frac{xk_{hnf}}{k_f\left(C_w - C_\infty\right)}\left.\frac{\partial C}{\partial y}\right|_{y=0}$$
$$C_{fx}\mathrm{Re}_x^{\frac{1}{2}} = \frac{1}{\left(1 - \phi_{MWCNT} - \phi_{Fe_3O_4}\right)^{2.5}} f''(0), \mathrm{Nu}_x\mathrm{Re}_x^{\frac{1}{2}} = -\left(\frac{k_{hnf}}{k_f} + \frac{4}{3}R\right)\theta'(0), \mathrm{Sh}_x\mathrm{Re}_x^{\frac{1}{2}} = -\left(\frac{k_{hnf}}{k_f}\right)\Phi'(0)$$

## Numerical solution

The nonlinear ODEs (7)–(10) are solved numerically by employing Runge–Kutta fourth-order method along with shooting technique. In this process, boundary value problem (BVP) is transformed to initial value problem (IVP). At first, the highest order terms can be written in the remaining lower-order terms as follows:

$$f''' = \frac{1}{\zeta_1\zeta_2}\left[-ff'' + 2f'^2 + \zeta_2\zeta_3 Mf' + \zeta_1\zeta_2 Kpf'\right], \tag{11}$$

$$\theta'' = \frac{-\Pr}{\zeta_4\left\{\frac{k_{hnf}}{k_f} + \frac{4}{3}R\right\}}\left[f\theta' - f'\theta + \zeta_4 q\theta\right], \tag{12}$$

$$\Phi'' = -\mathrm{Sc}\left[f\Phi' - f'\Phi - \mathrm{Kc}\Phi\right]. \tag{13}$$

Then, the governing equations are transformed to a set of following first ODEs by presenting the new variables as:

$$f = y_1, f' = y_2, f'' = y_3, \theta = y_4,\ \theta' = y_5, \Phi = y_6,\ \Phi' = y_7. \tag{14}$$

Let $y = \left[f\ f'\ f''\ \theta\ \theta'\ \Phi\ \Phi'\right]^T$ which gives

**Table 1** Comparison of $-\theta'(0)$ for base fluid $\left(\phi_{\mathrm{MWCNT}}=0, \phi_{\mathrm{Fe_3O_4}}=0\right)$ for various values of Pr

| Pr | Devi and Devi [46] | Waini et al. [47] | Present study | % error [46] | % error [47] |
|---|---|---|---|---|---|
| 2 | 0.91135 | 0.911357 | 0.91138216 | 0.00387 | 0.00276 |
| 6.13 | 1.75968 | 1.759682 | 1.75969204 | 0.00068 | 0.00057 |
| 7 | 1.89540 | 1.895400 | 1.89543144 | 0.00165 | 0.00165 |
| 20 | 3.35390 | 3.353893 | 3.35393720 | 0.00110 | 0.00131 |

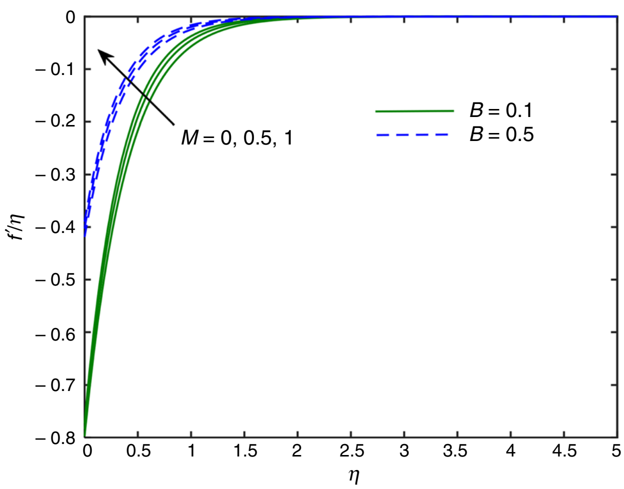


**Fig. 2** Variation in $f'(\eta)$ with $M$ and $B$

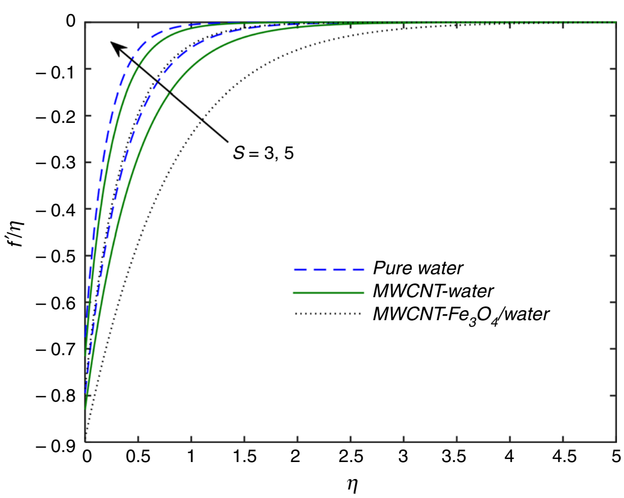


**Fig. 3** Variation in $f'(\eta)$ with $S$

$$\frac{\mathrm{d}}{\mathrm{d}\eta}\begin{bmatrix} y_1 \\ y_2 \\ y_3 \\ y_4 \\ y_5 \\ y_6 \\ y_7 \end{bmatrix} = \begin{bmatrix} y_2 \\ y_3 \\ \frac{1}{\zeta_1\zeta_2}\left[-y_1y_3 + 2y_2^2 + \zeta_2\zeta_3 M y_2 + \zeta_1\zeta_2 Kp y_2\right] \\ y_4 \\ \frac{-\mathrm{Pr}}{\zeta_4\left\{\frac{k_{\mathrm{hnf}}}{k_{\mathrm{f}}}+\frac{4}{3}R\right\}}\left[y_1y_5 - y_2y_4 + \zeta_4 q y_4\right] \\ y_6 \\ -\mathrm{Sc}\left[y_1y_7 - y_2y_6 - \mathrm{Kc}y_6\right] \end{bmatrix}, \tag{15}$$

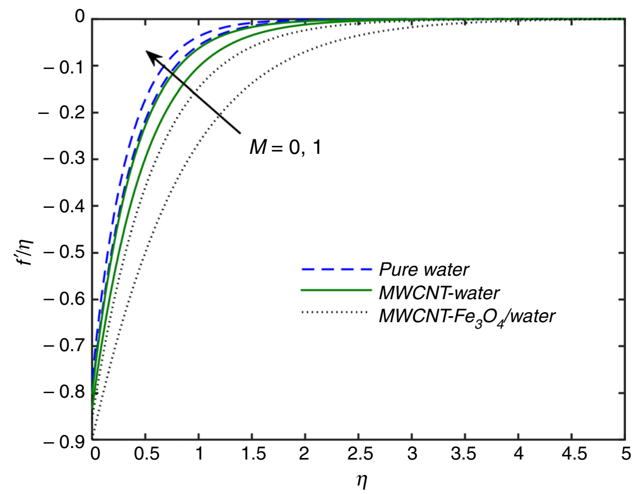


**Fig. 4** Variation in $f'(\eta)$ with $M$

subject to the initial conditions

$$\begin{aligned} &y_1(0) = S,\ y_2(0) = -1 + By_3(0),\ \ y_2(\infty) \to 0,\ y_3(0) = l_1, \\ &y_4(0) = 1 + Dy_5,\ \ y_4(\infty) \to 0, y_5(0) = l_2, \\ &y_6(0) = 1 + Ey_7,\ \ y_6(\infty) \to 0,\ y_7(0) = l_3, \end{aligned} \tag{16}$$

with some initial guess values of $l_1$, $l_2$, and $l_3$, we apply Runge–Kutta method of fourth order to solve the above IVP. There is an inbuilt self-corrective procedure in the MATLAB coding to correct the unknown guess values. Once the corrected values are attended, then the step-by-step integration by Runge–Kutta scheme is executed and the solution is attained within the prescribed error limit. The reduced Nusselt number $\left\{-\theta'(0)\right\}$ is compared with the works of Devi and Devi [58] and Waini et al. [59] in the absence of nanoparticles for different values of Pr, and results are in good agreement as shown in Table 1.

## Numerical results and discussion

The system of nonlinear ODEs (7)–(10) are solved numerically using the bvp4c scheme from MATLAB software to observe the influences of the related operating parameters in the flow domain. The impacts of such parameters are depicted clearly in Figs. 2–11. Table 2 provides the

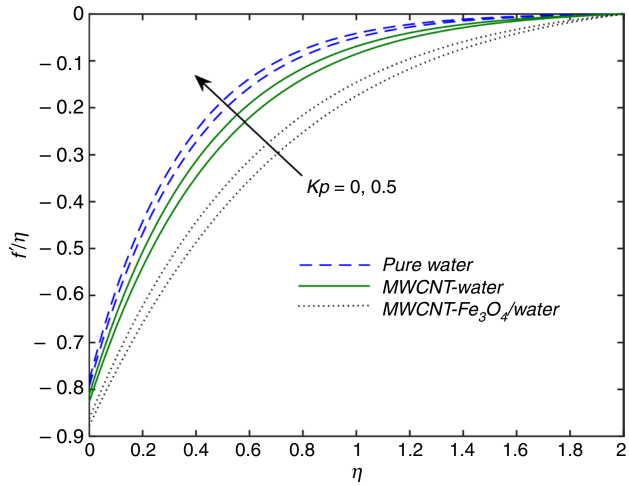


**Fig. 5** Variation in $f'(\eta)$ with $Kp$

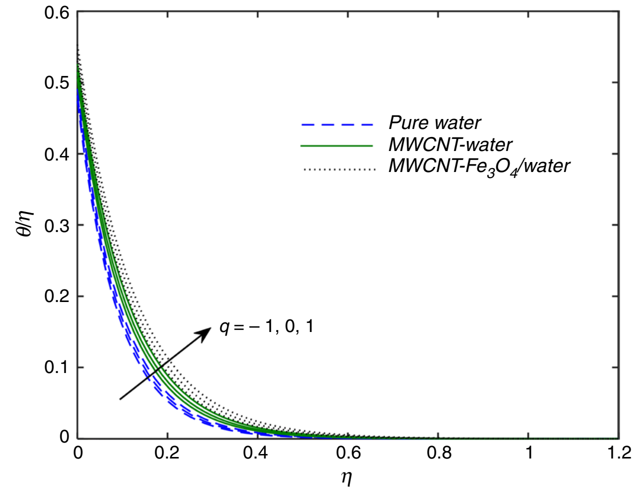


**Fig. 7** Variation in $\theta(\eta)$ with $q$

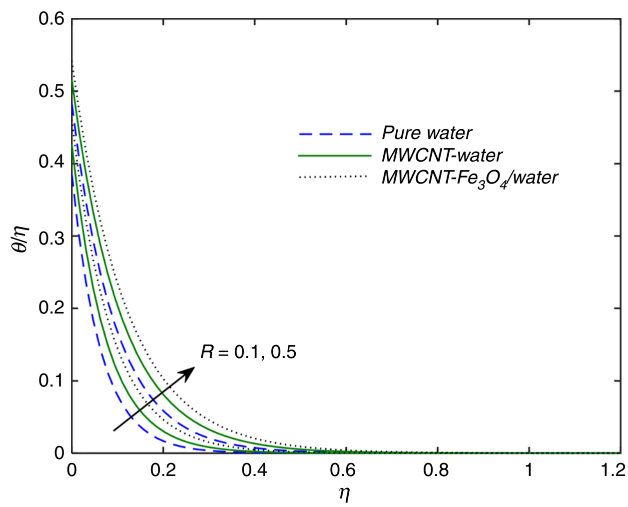


**Fig. 6** Variation in $\theta(\eta)$ with $R$

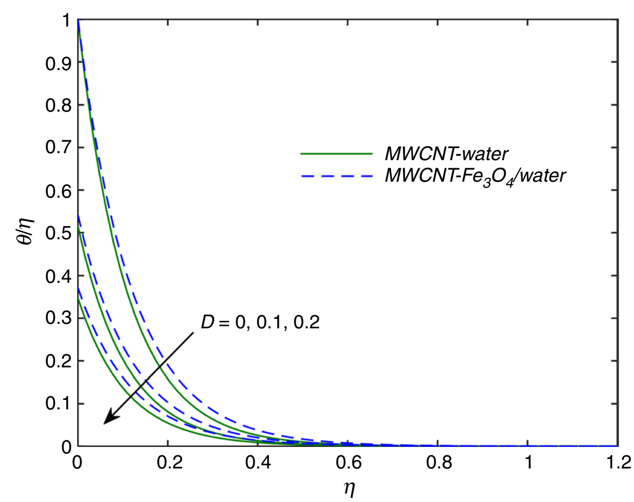


**Fig. 8** Variation in $\theta(\eta)$ with $D$

thermo-physical properties of base fluid and nanofluid at 25 °C. In the present study, we consider $\phi_1 = \phi_2 = 0$ for base fluid and $\phi_1 = \phi_2 = 0.05$ for hybrid nanofluid. During numerical simulations, we fixed the values of the parameters as $M = q = B = D = E = 0.1, \mathrm{Pr} = 6.2, \mathrm{Sc} = 0.6, \mathrm{Kp} = R = \mathrm{Kc} = 0.5$ and $S = 3$, unless otherwise the values are mentioned.

Figure 2 depicts the effects of magnetic parameter ($M$) and velocity slip parameter ($B$). It is seen that the velocity profiles $\left(f'(\eta)\right)$ increase due to rise in $M$ and $B$. Therefore, the velocity boundary layer thickness declines. Figure 3 presents the comparison of $f'(\eta)$ for $H_2O$, *MWCNT*–water and *MWCNT*-$Fe_3O_4$*/water* for various values of suction parameter ($S$). It is observed that $f'(\eta)$ increases for all types of fluids taken into consideration because suction reduces the drag on bodies in an external flow. Moreover, in a porous medium, the continuous suction is more effective than in a non-porous medium. This is the practical importance of combined effect of suction and porous medium. Further, it is seen that velocity of *MWCNT*-$Fe_3O_4$*/water* is lower than *MWCNT-water* and $H_2O$. Figure 4 depicts the comparison of velocity profiles due to absence and presence of magnetic parameter ($M$). When $M = 0$, the velocity of the all fluids is less than that of $M = 1$. Close analysis reveals that the velocity of the hybrid nanofluid is less than other fluids when $M = 0$. Figure 5 displays the effect of resistive force caused by the porous medium. A comparison study is made to analyze the effect of permeability parameter ($Kp$) on $f'(\eta)$ for $H_2O$, *MWCNT*–water and *MWCNT*-$Fe_3O_4$/water. It is perceived that $f'(\eta)$ of hybrid nanofluid is less in the absence of porous matrix.

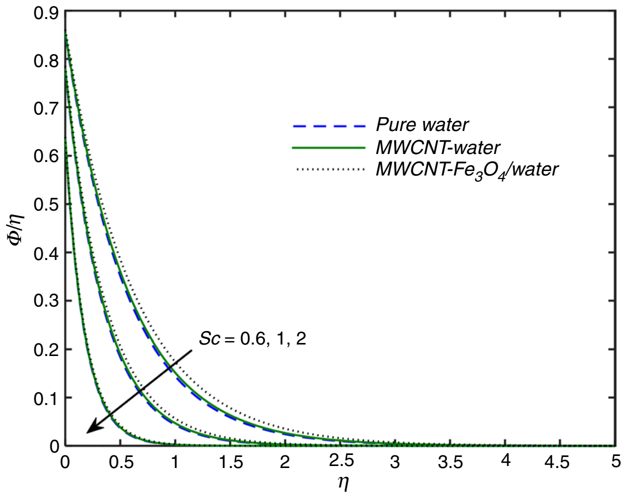


**Fig. 9** Variation in $\Phi(\eta)$ with Sc

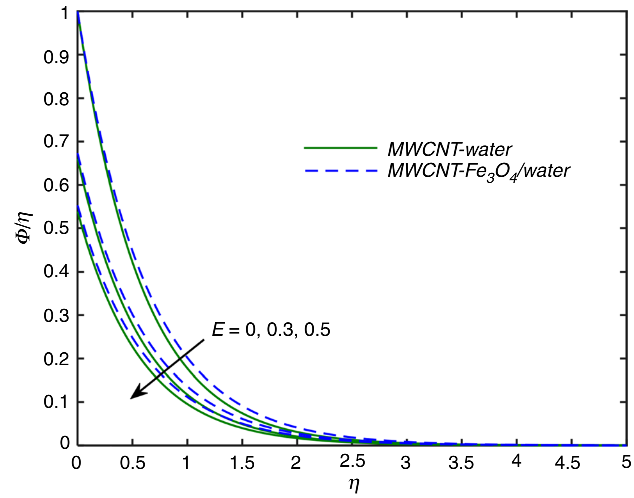


**Fig. 11** Variation in $\Phi(\eta)$ with $E$

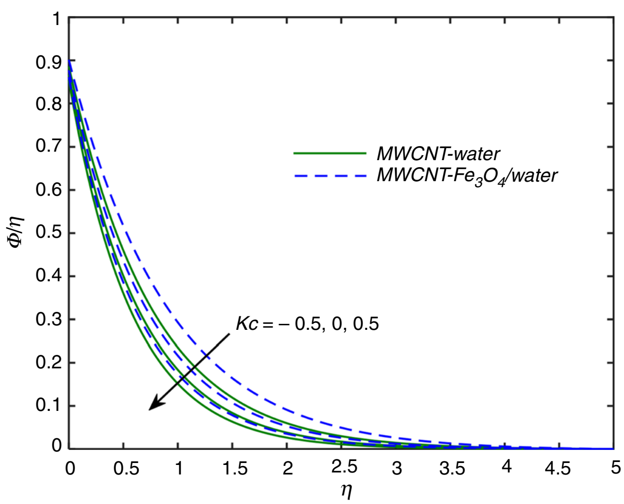


**Fig. 10** Variation in $\Phi(\eta)$ with $Kc$

**Table 2** Thermo-physical properties of MWCNT and $Fe_3O_4$ [29]

| Properties | $\rho/\text{kg m}^{-3}$ | $c_p/\text{kg}^{-1}\text{ K}^{-1}$ | $k/\text{W mK}^{-1}$ | $\sigma/\text{s m}^{-1}$ |
|---|---|---|---|---|
| Water $(H_2O)$ | 997.1 | 4179 | 0.613 | $5.5 \times 10^{-6}$ |
| MWCNT | 2100 | 711 | 3000 | $10^{-7}$ |
| $Fe_3O_4$ | 5810 | 670 | 6 | 25,000 |

**Table 3** Computation of $f''(0)$ for nanofluid (*MWCNT*–water) and hybrid nanofluid (*MWCNT-Fe$_3$O$_4$*/water) when $D=E=q=0.1$, $\Pr=6.2$, $\text{Sc}=0.6$, $R=Kc=0.5$

| $M$ | $Kp$ | $B$ | $S$ | $\frac{1}{(1-\phi_{\text{MWCNT}})^{2.5}}f''(0)$ | $\frac{1}{\left(1-\phi_{\text{MWCNT}}-\phi_{\text{Fe}_3\text{O}_4}\right)^{2.5}}f''(0)$ |
|---|---|---|---|---|---|
| 0 | 0 | 0.1 | 3 | 1.92854350 | 1.54161210 |
| 0.5 | 0 | 0.1 | 3 | 2.10840999 | 1.75307917 |
| 1 | 0 | 0.1 | 3 | 2.25471041 | 1.92321203 |
| 1 | 0.5 | 0.1 | 3 | 2.37695138 | 2.06342649 |
| 1 | 1 | 0.1 | 3 | 2.48409754 | 2.18560075 |
| 1 | 1 | 0.3 | 3 | 1.76097100 | 1.67726982 |
| 1 | 1 | 0.5 | 3 | 1.35381381 | 1.34804675 |
| 1 | 1 | 0.5 | 5 | 1.57245114 | 1.60778222 |
| 1 | 1 | 0.5 | 7 | 1.71096993 | 1.78428674 |

Figure 6 represents the comparison of temperature profiles $\theta(\eta)$ between hybrid nanofluid (*MWCNT-Fe$_3$O$_4$/*water), nanofluid (*MWCNT*–water) and base fluid (water) by the inspiration of radiation parameter ($R$). It is perceived that under same conditions, the hybrid nanofluid achieves higher temperature than nanofluid and regular fluid. In general, $\theta(\eta)$ is an increasing function of $R$. For higher values of $R$ (i.e., thermal radiation is dominate over conduction), an excessive amount of heat energy is released due to radiation which increases $\theta(\eta)$. Figure 7 reveals that heat source/sink parameter ($q$) enhances $\theta(\eta)$. From Fig. 8, it is found that the thermal slip parameter ($D$) causes a decline in $\theta(\eta)$. Moreover, temperature of *MWCNT–Fe$_3$O$_4$*/water is more higher than that of *MWCNT*–water and water.

Figure 9 shows the effect of Schmidt number (Sc) on concentration distribution $\Phi(\eta)$. Since Sc is the ratio of momentum diffusivity and mass diffusivity, heavier species leads to reduce $\Phi(\eta)$. Further,$\Phi(\eta)$ for hybrid nanofluid (*MWCNT–Fe$_3$O$_4$*/water), nanofluid (*MWCNT*/water) and base fluid (water) are almost same. Figure 10 depicts the effects of $Kc$ on concentration profiles $\Phi(\eta)$. Here $Kc > 0$ relates to constructive and $Kc < 0$ for destructive chemical reaction. It is seen that higher values of $Kc$ diminish the

**Table 4** Computation of $-\theta'(0)$ and $-\Phi'(0)$ for nanofluid (*MWCNT*–water) and hybrid nanofluid ($MWCNT–Fe_3O_4$/water) when $M=B=q=0.1$, $Kp=0.5$, $S=3$

| $D$ | $E$ | Pr | $R$ | Sc | $Kc$ | $-\left(\frac{k_{nf}}{k_f}+\frac{4}{3}R\right)\theta'(0)$ | $-\left(\frac{k_{hnf}}{k_f}+\frac{4}{3}R\right)\theta'(0)$ | $-\left(\frac{\kappa_{nf}}{\kappa_f}\right)\Phi'(0)$ | $-\left(\frac{\kappa_{hnf}}{\kappa_f}\right)\Phi'(0)$ |
|---|---|---|---|---|---|---|---|---|---|
| 0.1 | 0.1 | 6.2 | 0.1 | 0.6 | 0.5 | 7.39314713 | 7.88242826 | 1.74720315 | 1.95546112 |
| 0.3 | 0.1 | 6.2 | 0.1 | 0.6 | 0.5 | 3.44359286 | 3.79295417 | 1.74720315 | 1.95546112 |
| 0.5 | 0.1 | 6.2 | 0.1 | 0.6 | 0.5 | 2.24452604 | 2.49732150 | 1.74720315 | 1.95546112 |
| 0.5 | 0.3 | 6.2 | 0.1 | 0.6 | 0.5 | 2.24452604 | 2.49732150 | 1.34161125 | 1.51081354 |
| 0.5 | 0.5 | 6.2 | 0.1 | 0.6 | 0.5 | 2.24452604 | 2.49732150 | 1.08884838 | 1.23091806 |
| 0.5 | 0.5 | 7 | 0.1 | 0.6 | 0.5 | 2.27930036 | 2.54146156 | 1.08884838 | 1.23091806 |
| 0.5 | 0.5 | 10 | 0.1 | 0.6 | 0.5 | 2.36339086 | 2.64850567 | 1.08884838 | 1.23091806 |
| 0.5 | 0.5 | 10 | 0.5 | 0.6 | 0.5 | 3.22624495 | 3.48967989 | 1.08884838 | 1.23091806 |
| 0.5 | 0.5 | 10 | 1 | 0.6 | 0.5 | 4.22160199 | 4.45866176 | 1.08884838 | 1.23091806 |
| 0.5 | 0.5 | 10 | 1 | 1 | 0.5 | 4.22160199 | 4.45866176 | 1.36292397 | 1.55099536 |
| 0.5 | 0.5 | 10 | 1 | 2 | 0.5 | 4.22160199 | 4.45866176 | 1.71693525 | 1.96760703 |
| 0.5 | 0.5 | 10 | 1 | 2 | 0.3 | 4.22160199 | 4.45866176 | 1.71133036 | 1.96079363 |
| 0.5 | 0.5 | 10 | 1 | 2 | 0 | 4.22160199 | 4.45866176 | 1.70242284 | 1.94991787 |
| 0.5 | 0.5 | 10 | 1 | 2 | −0.3 | 4.22160199 | 4.45866176 | 1.69283327 | 1.93813746 |
| 0.5 | 0.5 | 10 | 1 | 2 | −0.5 | 4.22160199 | 4.45866176 | 1.68600645 | 1.92970072 |

concentration level in all the layers. Figure 11 shows the effect of solutal slip parameter ($E$) on $\Phi(\eta)$. It is observed that the higher values of $E$ decrease $\Phi(\eta)$ for both nanofluid and hybrid nanofluid.

Table 3 is computed to observe the impact of $M$, $Kp$, $B$ and $S$ on skin friction coefficients for nanofluid (*MWCNT*/water) and hybrid nanofluid ($MWCNT–Fe_3O_4$/water). It is seen that $M$, $Kp$ and $S$ enhance the skin friction coefficients, but reverse effect is seen for $B$. Table 4 is calculated to get the impact of operating parameters such as $D$, $E$, Pr, $R$, Sc, and $Kc$ on local Nusselt number and local Sherwood number for nanofluid and hybrid nanofluid. It is perceived that $D$, Pr, and $R$ are responsible for heat transfer rate, whereas $E$, Sc, and $Kc$ are responsible for mass transfer. Greater values of Pr and $R$ boost the local Nusselt number, but $D$ reduces it. In similar way, Sc and $Kc$ increase the local Sherwood number and $E$ decreases it. It is interesting to note that $E$, Sc, and $Kc$ have no impact on local Nusselt number and $D$, $Pr$, and $R$ have no inspiration on local Sherwood number.

## Conclusions

The key findings of the current study are:

- Hybridity enhances the temperature profiles as well as concentration profiles.
- Slip parameters are responsible to decrease their respective profiles.
- Sc and $Kc$ boost the mass transfer rate, whereas Pr and $R$ enhance the heat transfer rate.
- There is an improvement in shearing stress at the wall by augmenting the values of $M$, Kp, and $S$.

Finally, it is concluded that the external new parameters such as Slip parameters, Schmidt number, chemical reaction, Prandtl number, and radiation make a significant impact on the hybridity which enriches the temperature and concentration profiles.

## Compliance with ethical standards

**Conflict of interest** The authors declare that they have no conflict of interest.

## References


1. Fang T, Zhang J. Closed-form exact solution of MHD viscous flow over a shrinking sheet. Commun Nonlinear Sci Numer Simul. 2009;14:2853–7.
2. Bhattacharyya K. Boundary layer flow and heat transfer over an exponentially shrinking sheet. Chin Phys Lett. 2011;28(7):074701.
3. Mukhopadhyay S. MHD boundary layer flow and heat transfer over an exponentially stretching sheet embedded in a thermally stratified medium. Alex Eng J. 2013;52:259–65.
4. Nadeem S, Ul Haq R, Khan ZH. Heat transfer analysis of water-based nanofluid over an exponentially stretching sheet. Alex Eng J. 2014;53:219–24.
5. Swain K, Parida SK, Dash GC. MHD flow of viscoelastic nanofluid over a stretching sheet in a porous medium with heat source and chemical reaction. Annales de Chimie- Science des Matériaux. 2018;42(1):7–21.
6. Motsumi TG, Makinde OD. Effects of thermal radiation and viscous dissipation on boundary layer flow of nanofluids over a permeable moving flat plate. Phys Scr. 2012;86:045003. https://doi.org/10.1088/0031-8949/86/04/045003.

7. Naramgari S, Sulochana C. MHD flow over a permeable stretching/shrinking sheet of a nanofluid with suction/injection. Alex Eng J. 2016;55:819–27.
8. Swain K, Parida SK, Dash GC. Higher order chemical reaction on MHD nanofluid flow with slip boundary conditions: a numerical approach. Math Modell Eng Probl. 2019;6(2):293–9.
9. Hady FM, Ibrahim FS, Abdel-Gaied SM, Eid MR. Radiation effect on viscous flow of a nanofluid and heat transfer over a nonlinearly stretching sheet. Nanoscale Res Lett. 2012;7(229):1–13.
10. Sheikholeslami M, Abelman S, Ganji DD. Numerical simulation of MHD nanofluid flow and heat transfer considering viscous dissipation. Int J Heat Mass Transf. 2014;79:212–22.
11. Mahanthesh B, Gireesha BJ, Reddy Gorla RS. Nonlinear radiative heat transfer in MHD three-dimensional flow of water based nanofluid over a non-linearly stretching sheet with convective boundary condition. J Niger Math Soc. 2016;35:178–98.
12. Ghosh S, Mukhopadhyay S. Viscous flow due to an exponentially shrinking permeable sheet in nanofluid in presence of slip. Int J Comput Methods Eng Sci Mech. 2017;18:309–17.
13. Mebarek-Oudina F. Convective heat transfer of Titania nanofluids of different base fluids in cylindrical annulus with discrete heat source. Heat Transf Asian Res. 2019;48(1):135–47. https://doi.org/10.1002/htj.21375.
14. Kolsi L, Oztop HF, Ghachem K, Almeshaal MA, Mohammed H, Babazadeh H, Abu-Hamdeh N. Numerical study of periodic magnetic field effect on 3D natural convection of MWCNT-water/nanofluid with consideration of aggregation. Processes. 2019;7(957):1–21.
15. Ghosh S, Mukhopadhyay S. Stability analysis for model-based study of nanofluid flow over an exponentially shrinking permeable sheet in presence of slip. Neural Comput Appl. 2019. https://doi.org/10.1007/s00521-019-04221-w.
16. Gourari S, Mebarek-Oudina F, Hussein AK, Kolsi L, Hassen W, Younis O. Numerical study of natural convection between two coaxial inclined cylinders. Int J Heat Technol. 2019;37(3):779–86.
17. Raza J, Farooq M, Mebarek-Oudina F, Mahanthesh B. Multiple slip effects on MHD non-Newtonian nanofluid flow over a nonlinear permeable elongated sheet: numerical and statistical analysis. Multidiscip Model Mater Struct. 2019;15(5):913–31.
18. Mebarek-Oudina F, Bessaïh R. Numerical simulation of natural convection heat transfer of copper-water nanofluid in a vertical cylindrical annulus with heat sources. Thermophys Aeromech. 2019;26(3):325–34.
19. Zaim A, Aissa A, Mebarek-Oudina F, Mahanthesh B, Lorenzini G, Sahnoun M, El Ganaoui M. Galerkin finite element analysis of magneto-hydrodynamic natural convection of Cu-water nanoliquid in a baffled U-shaped enclosure. Propuls Power Res. 2020. https://doi.org/10.1016/j.jppr.2020.10.002.
20. Farhan M, Omar Z, Mebarek-Oudina F, Raza J, Shah Z, Choudhari RV, Makinde OD. Implementation of one step one hybrid block method on nonlinear equation of the circular sector oscillator. Comput Math Model. 2020;31:116–32.
21. Marzougui S, Mebarek-Oudina F, Aissa A, Magherbi M, Shah Z, Ramesh K. Entropy generation on magneto-convective flow of copper-water nanofluid in a cavity with chamfers. J Therm Anal Calorim. 2020. https://doi.org/10.1007/s10973-020-09662-3.
22. Laouira H, Mebarek-Oudina F, Hussein AK, Kolsi L, Merah A, Younis O. Heat transfer inside a horizontal channel with an open trapezoidal enclosure subjected to a heat source of different lengths. Heat Transf Asian Res. 2020;49(1):406–23. https://doi.org/10.1002/htj.21618.
23. Zaim A, Aissa A, Mebarek-Oudina F, Rashad AM, Hafiz MA, Sahnoun M, El Ganaoui M. Magnetohydrodynamic natural convection of hybrid nanofluid in a porous enclosure: numerical analysis of the entropy generation. J Therm Anal Calorim. 2020;141(5):1981–92. https://doi.org/10.1007/s10973-020-09690-z.
24. Khan U, Zaib A, Mebarek-Oudina F. Mixed convective magneto flow of $SiO_2$–$MoS_2/C_2H_6O_2$ hybrid nanoliquids through a vertical stretching/shrinking wedge: stability analysis. Arab J Sci Eng. 2020;45(11):9061–73. https://doi.org/10.1007/s13369-020-04680-7.
25. Swain K, Mahanthesh B, Mebarek-Oudina F. Heat transport and stagnation-point flow of magnetized nanoliquid with variable thermal conductivity with Brownian moment and thermophoresis aspects. Heat Transf. 2020. https://doi.org/10.1002/htj.21902.
26. Mebarek-Oudina F, Bessaih R, Mahanthesh B, Chamkha AJ, Raza J. Magneto-thermal-convection stability in an inclined cylindrical annulus filled with a molten metal. Int J Numer Methods Heat Fluid Flow. 2020. https://doi.org/10.1108/HFF-05-2020-0321.
27. Hayat T, Nadeem S. Heat transfer enhancement with Ag–CuO/water hybrid nanofluid. Results Phys. 2017;7:2317–24.
28. Ghadikolaei SS, Hosseinzadeh K, Ganji DD. Investigation on ethylene glycol-water mixture fluid suspend by hybrid nanoparticles ($TiO_2$–CuO) over rotating cone with considering nanoparticles shape factor. J Mol Liq. 2018;272:226–36. https://doi.org/10.1016/j.molliq.2018.09.084.
29. Waini I, Ishak A, Pop I. Hybrid nanofluid flow and heat transfer over a nonlinear permeable stretching/shrinking surface. Int J Numer Methods Heat Fluid Flow. 2019;29:3110–27. https://doi.org/10.1108/HFF-01-2019-0057.
30. Bagheri H, Behrang M, Assareh E, Izadi M, Sheremet MA. Free convection of hybrid nanofluids in a C-shaped chamber under variable heat flux and magnetic field: simulation, sensitivity analysis, and artificial neural networks. Energies. 2019;12:1–17. https://doi.org/10.3390/en12142807.
31. Ali Lunda L, Omara Z, Khan I, Seikh A, El-Sayed H, Sherif M, Nisar KS. Stability analysis and multiple solution of Cu–$Al_2O_3$/$H_2O$ nanofluid contains hybrid nanomaterials over a shrinking surface in the presence of viscous dissipation. J Matter Res Technol. 2020;9(1):421–32.
32. Aziz A, Jamshed W, Ali Y, Shams M. Heat transfer and entropy analysis of Maxwell hybrid nanofluid including effects of inclined magnetic field, Joule heating and thermal radiation. Discrete Contin Dyn Syst Ser S. 2020. https://doi.org/10.3934/dcdss.2020142.
33. Ali Lunda L, Omara Z, Khan I, Sherif ESM. Dual solutions and stability analysis of a hybrid nanofluid over a stretching/shrinking sheet executing MHD flow. Symmetry. 2020;12:276. https://doi.org/10.3390/sym12020276.
34. Raza J, Mebarek-Oudina F, Ram P, Sharma S. MHD flow of non-Newtonian molybdenum disulfide nanofluid in a converging/diverging channel with Rosseland radiation. Defect Diffus Forum. 2020;401:92–106. https://doi.org/10.4028/www.scientific.net/DDF.401.92.
35. Mebarek-Oudina F, Makinde OD. Numerical simulation of oscillatory MHD natural convection in cylindrical annulus Prandtl number effect. Defect Diffus Forum. 2018;387:417–27. https://doi.org/10.4028/www.scientific.net/DDF.387.417.
36. Mebarek-Oudina F, Aissa A, Mahanthesh B, Öztop FH. Heat transport of magnetized newtonian nanoliquids in an annular space between porous vertical cylinders with discrete heat source. Int Commun Heat Mass Transf. 2020;117:104737. https://doi.org/10.1016/j.icheatmasstransfer.2020.104737.
37. Hamrelaine S, Mebarek-Oudina F, Sari MR. Analysis of MHD Jeffery Hamel flow with suction/injection by homotopy analysis method. J Adv Res Fluid Mech Therm Sci. 2019;58(2):173–86.
38. Mebarek-Oudina F. Numerical modeling of the hydrodynamic stability in vertical annulus with heat source of different lengths. Eng Sci Technol. 2017;20(4):1324–33. https://doi.org/10.1016/j.jestch.2017.08.003.

39. Mebarek-Oudina F, Keerthi Reddy N, Sankar M. Heat source location effects on buoyant convection of nanofluids in an annulus. Adv Fluid Dyn. https://doi.org/10.1007/978-981-15-4308-1_70.
40. Abo-Dahab SM, Abdelhafez MA, Mebarek-Oudina F, Bilal SM. MHD casson nanofluid flow over nonlinearly heated porous medium in presence of extending surface effect with suction/injection. Indian J Phys. 2020. https://doi.org/10.1007/s12648-020-01923-z.
41. Sundar LS, Singh MK, Sousa ACM. Enhanced heat transfer and friction factor of MWCNT–Fe3$O_4$/water hybrid nanofluids. Int Commun Heat Mass Transf. 2020;52:73–83.
42. Sohail M, Naz R, Abdelsalam SI. On the onset of entropy generation for a nanofluid with thermal radiation and gyrotactic microorganisms through 3D flows. Phys Scr. 2020;95:045206.
43. Sohail M, Raza R. Analysis of radiative magneto nano pseudoplastic material over three dimensional nonlinear stretched surface with passive control of mass flux and chemically responsive species. Multidiscip Model Mater Struct. 2020. https://doi.org/10.1108/MMMS-08-2019-0157.
44. Sohail M, Naz R. Modified heat and mass transmission models in the magnetohydrodynamic flow of Sutter by nanofluid in stretching cylinder. Phys A. 2020;549:124088.
45. Sohail M, Naz R, Abdelsalam SI. Application of non-Fourier double diffusions theories to the boundary-layer flow of a yield stress exhibiting fluid model. Phys A. 2020;537:122753.
46. Sohail M, Naz R, Bilal S. Thermal performance of an MHD radiative Oldroyd-B nanofluid by utilizing generalized models for heat and mass fluxes in the presence of bioconvective gyrotactic microorganisms and variable thermal conductivity. Heat Transf Asian Res. 2019;48:1–17.
47. Shah Z, Hajizadeh MR, Alreshidi NA, Deebani W, Shutaywi M. Entropy optimization and heat transfer modeling for Lorentz forces effect on solidification of NEPCM. Int Commun Heat Mass Transf. 2020;117:104715.
48. Shah Z, Kumam P, Deebani W. Radiative MHD Casson nanofuid flow with activation energy and chemical reaction over past nonlinearly stretching surface through entropy generation. Sci Rep. 2020;10:4402.
49. Wakif A. A novel numerical procedure for simulating steady MHD convective flows of radiative Casson fluids over a horizontal stretching sheet with irregular geometry under the combined influence of temperature-dependent viscosity and thermal conductivity. Math Probl Eng. 2020; Article ID 1675350.
50. Shah Z, Dawar A, Khan I, Islam S, Ching DLC, Khan AZ. Cattaneo-Christov model for electrical magnetite micropolar Casson ferrofluid over a stretching/shrinking sheet using effective thermal conductivity model. Case Stud Therm Eng. 2019;13:100352.
51. Shah Z, Islam S, Ayaz H, Khan S. Radiative heat and mass transfer analysis of micropolar nanofluid flow of Casson fluid between two rotating parallel plates with effects of hall current. J Heat Transf. 2019;141(2):022401.
52. Deebani W, Tassaddiq A, Shah Z, Dawar A, Ali F. Hall effect on radiative Casson fluid flow with chemical reaction on a rotating cone through entropy optimization. Entropy. 2020. https://doi.org/10.3390/e22040480.
53. Senapati M, Swain K, Parida SK. Numerical analysis of three-dimensional MHD flow of Casson nanofluid past an exponentially stretching sheet. Karbala Int J Mod Sci. 2020;6:13. https://doi.org/10.33640/2405-609x.1462.
54. Wakif A, Chamkha A, Thumma T, Animasaun IL, Sehaqui R. Thermal radiation and surface roughness effects on the thermo-magneto-hydrodynamic stability of alumina-copper oxide hybrid nanofuids utilizing the generalized Buongiorno's nanofuid model. J Therm Anal Calorim. 2020. https://doi.org/10.1007/s10973-020-09488-z.
55. Wakif A, Boulahia Z, Mishra SR, Rashidi MM, Sehaqui R. Influence of a uniform transverse magnetic field on the thermo-hydrodynamic stability in water-based nanofluids with metallic nanoparticles using the generalized Buongiorno's mathematical model. Eur Phys J Plus. 2018;133:181. https://doi.org/10.1140/epjp/i2018-12037-7.
56. Wakif A, Qasim M, Afridi MI, Saleem S, Al-Qarni MM. Numerical examination of the entropic energy harvesting in a magneto-hydrodynamic dissipative flow of stokes' second problem: utilization of the gear-generalized differential quadrature method. J Non-Equilib Thermodyn. 2019. https://doi.org/10.1515/jnet-2018-0099.
57. Wakif A, Boulahia Z, Ali F, Eid MR, Sehaqui R. Numerical analysis of the unsteady natural convection MHD Couette nanofluid flow in the presence of thermal radiation using single and two-phase nanofluid models for Cu-water nanofluids. Int J Appl Comput Math. 2018;4:81. https://doi.org/10.1007/s40819-018-0513-y.
58. Devi SU, Devi SPA. Heat transfer enhancement of Cu–$Al_2O_3$/Water hybrid nanofluid flow over a stretching sheet. J Niger Math Soc. 2017;36(2):419–33.
59. Waini I, Ishak A, Pop I. Hybrid nanofluid flow and heat transfer past a permeable stretching/shrinking surface with a convective boundarycondition. J Phys Conf Ser. 2019;1366:012022. https://doi.org/10.1088/1742-6596/1366/1/012022.